

Evolution of ferromagnetic and nFL states with doping: the case of Ru doped UCoGe

Michal Vališka,^{1,*} Jiří Pospíšil,² Vladimír Sechovský,¹ and Martin Diviš¹

¹*Faculty of Mathematics and Physics, Charles University,
DCMP, Ke Karlovu 5, CZ-12116 Praha 2, Czech Republic*

²*Advanced Science Research Center, Japan Atomic Energy Agency, Tokai, Ibaraki, 319-1195, Japan*

We report on evolution of ferromagnetism (FM) and non-Fermi liquid (nFL) state in the Ru doped ferromagnetic superconductor UCoGe. We have detected that Ru substitution on the Co site in the UCoGe leads to an initial sharp increase of the Curie temperature up to the maximum of $T_C = 8.6$ K for $x \approx 0.1$ accompanied by spontaneous magnetic moment enhancement. On the other hand the superconducting state vanishes already by 3% of the Ru. Further increase of the Ru content beyond $x \approx 0.1$ leads to the suppression of both, T_C and the spontaneous magnetic moment, creating a well-developed ferromagnetic dome in the $T - x$ phase diagram. Concentration dependence of the critical exponents of the electrical resistivity and heat capacity together with the scaling of T_C has signs of the non-Fermi liquid behavior which suggests presence of the quantum critical point (QCP) near the critical concentration $x \approx 0.3$ where the ordering temperature is suppressed to zero. Detailed analysis of the critical exponents assigns the quantum phase transition most likely as a continuous Hertz-Millis type. We discuss the ferromagnetism development on the basis of band structure evolution. We support the scenario by results of electronic structure calculations and employment of the simplified periodic Anderson model.

PACS numbers: 71.10.Hf, 74.40.Kb, 71.20.Lp

Keywords: UCoGe, URuGe, Quantum critical point, non-Fermi liquid behavior, ferromagnetism

I. INTRODUCTION

The phenomena emerging near to the quantum critical points (QCP) belong to the most intensively studied topics of the condensed matter physics because research in this field has serious impacts on development of the new theoretical approaches for electron correlations in the materials. The research in this field is in continuous confrontation with the new coming materials carrying completely novel properties. Such intriguing materials are recently discovered uranium ferromagnetic superconductors (FM SC). This fascinating group has only three members – UGe₂¹, URhGe² and UCoGe³. Superconductivity and itinerant ferromagnetism are carried by the same uranium $5f$ electrons. It is a big novelty distinguishing them from previously reported ones like ZrZn₂⁴. UGe₂, the first discovered case, is a model example of the superconductivity (SC) induced by external pressure. The SC appears and reaches its maximum on a boundary between the two FM phases under the high pressure. URhGe and UCoGe are ambient pressure FM SC where both phenomena naturally coexist. Lot of scientific effort in both theoretical and experimental field has been already spent to understand this mutual coexistence of FM and SC. The ferromagnetic spin fluctuations which appear in the vicinity of the QCPs inducing unconventional spin triplet SC state have been considered as the main essence of the problem. QCP can be principally reached when a (magnetic) ordering temperature is suppressed to 0 K by changing of some external non-thermal control parameter such as pressure, magnetic field or chemical doping. Quantum phase transitions (QPTs) were experimentally studied for a broad spectrum of the materials like high- T_C superconductors⁵, ordinary metals⁶ or

heavy-fermion metals⁷. As the prominent examples one should mention CeCu_{6-x}Au_x with the antiferromagnetic quantum critical point (AF QCP) induced by chemical doping⁸ and YbRh₂Si₂ where AF QCP is achieved by applying external magnetic field⁹. In all these cases a second-order transition is reported showing continuous character. Nevertheless a ferromagnetic order in the compounds like the itinerant electron ferromagnets MnSi⁶ or UGe₂¹⁰ is suppressed to the zero temperature by external pressure showing signs of a first-order transition. It has to be mentioned, that these first-order phase transitions should not deserve to be marked as the QPTs according to the continuity requirement. However, such QPTs have to be treated as essentially different to the classical transitions which take place at nonzero temperatures. Thus discontinuous QPTs should be also taken into account and can in principle contribute to the investigation of the novel phases¹¹.

UCoGe, the subject of our research, is unique in the group of FM SC due to the much lower energy scale on which the magnetism appears¹². Curie temperature for UCoGe is only 3 K¹³ and together with the tiny spontaneous magnetic moment of $0.03 \mu_B$ indicates that UCoGe is close to a ferromagnetic instability¹⁴. It has been observed, however, that the Ru and Fe substitution for Co stabilizes the ferromagnetic state rapidly¹⁵, despite URuGe and UFeGe are paramagnetic down to the lowest temperatures¹⁶. Similar increase of T_C was reported also in the case of Co and Ru doped URhGe^{17,18}. In addition, it was experimentally proved that the non-Fermi liquid state develops on the boundary of the FM dome^{18,19}. It is evident that the region around the Co and Rh in the TiNiSi-type $UTGe$ compounds (T = transition metal) offers unique conditions for the quantum phase transitions

studies. This observation motivated us to study the development of the magnetism in the $\text{UCo}_{1-x}\text{Ru}_x\text{Ge}$ system for substitutions over a wide range of concentrations searching for the region of the inevitable disappearance of ferromagnetism where one may expect a ferromagnetic quantum critical point (FM QCP). We would like to test the type of this FM QCP, because the Co-Ru doping is not isoelectronic and in addition to it causes mixture of the 3d and 4d bands which significantly differentiate our work from previously done on $\text{URh}_{1-x}\text{Ru}_x\text{Ge}$ ²⁰. Influence of the substitutional disorder on development of the quantum phase phenomena will be also tested within our work. In the first stage an extensive investigation of structure, magnetization, magnetic susceptibility, specific heat and electrical resistance for numerous polycrystalline samples with various x has been performed.

II. EXPERIMENTAL DETAILS

In order to study the development of the magnetic state in the $\text{UCo}_{1-x}\text{Ru}_x\text{Ge}$ system we have primarily prepared a series of the polycrystalline samples with different concentration of the Ru for x going from 0 to 0.9. All samples were prepared by arc-melting of the stoichiometric amounts of the elements (purity of Co 4N5, Ge 6N and Ru 3N5). We used the U purified by Solid State Electrotransport technique (SSE)²¹ following previous experiences with preparation of UCoGe ²¹. The arc melting process was realized under protective Ar (6N purity) atmosphere on a water cooled Cu crucible. Each sample was three times turned upside down and subsequently re-melted in order to achieve the best homogeneity. No sign of evaporation was observed during the melting. Resulting masses of our samples were typically 2.5 g. All samples were separately wrapped into a Ta foil (99.99%) and sealed in a quartz tube under the vacuum of $1 \cdot 10^{-6}$ mbar and subsequently annealed at 885 °C for 14 days and then slowly cooled down to room temperature to avoid creation of the internal stresses. Each sample was characterized by X-ray powder diffraction (XRPD) at room temperature on a Bruker D8 Advance diffractometer. The obtained data were evaluated by standard Rietveld technique²² using FullProf/WinPlotr software^{23,24} with respect to the previously published crystallographic data of the UCoGe ²⁵ and URuGe ¹⁶ compound. Chemical composition of our samples was verified by scanning electron microscope (SEM) Tescan Mira I LMH equipped by an energy dispersive X-ray detector (EDX) Bruker AXS. Samples were afterward properly shaped for individual measurements with a fine wire saw to prevent additional stresses. Bar-shaped samples ($1 \times 0.5 \times 4 \text{ mm}^3$) were used for the low temperature resistivity measurements performed on a PPMS14T (Quantum Design) with the ^3He insert down to 350 mK. Heat capacity measurements were performed on the thin plates ($2 \times 2 \times 0.2 \text{ mm}^3$) using relaxation method on the PPMS9T and PPMS14T devices using

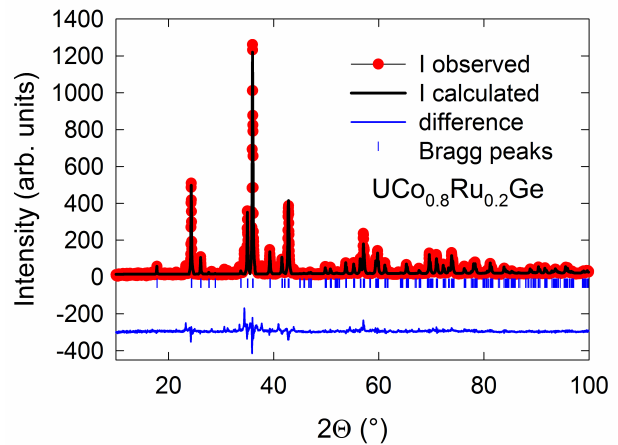


FIG. 1. (Color online) - Representative XRPD pattern of the $\text{UCo}_{0.8}\text{Ru}_{0.2}\text{Ge}$ compound. Red points refers to measured intensities, black bold line is calculated pattern, blue thin line is difference and vertical bars are positions of the Bragg peaks.

the same ^3He insert. Magnetization measurements were done on the roughly cubic samples ($2 \times 2 \times 2 \text{ mm}^3$) in a MPMS7T device. The density of states calculations were performed on the basis of the density-functional theory (DFT) within the local-spin-density approximation (LSDA)²⁶ and the generalized gradient approximation (GGA)²⁷. We used the full-potential augmented-plane-wave together with the local-orbitals method (APW+lo) as a part of the latest version (WIEN2k) of the original WIEN code²⁸ for this calculations.

III. RESULTS

UCoGe and URuGe both possess the orthorhombic TiNiSi structure (space group Pnma)^{16,25} with the cell parameters $a = 6.852 \text{ \AA}$, $b = 4.208 \text{ \AA}$, $c = 7.226 \text{ \AA}$ and $a = 6.678 \text{ \AA}$, $b = 4.359 \text{ \AA}$, $c = 7.539 \text{ \AA}$, respectively^{16,25}. Thus the unit cell volume of the ferromagnetic UCoGe is smaller ($V = 208.3 \text{ \AA}^3$)²⁵ of about 5% than the URuGe compound ($V = 219.5 \text{ \AA}^3$)¹⁶. XRPD patterns confirmed orthorhombic TiNiSi -type structure in the whole series of the doped materials. Typically all reflections could be assigned to the expected TiNiSi structure. One representative XRPD pattern is displayed in Fig. 1.

The evaluated lattice parameters of the Ru doped samples are shown with respect to increasing Ru concentration in Fig. 2. The concentration dependence of all three lattice parameters and also the unit cell volume is linear, i.e. obey the Vegard's law²⁹ (see Table I).

While the b and c lattice parameters increase with the increasing x the lattice parameter a simultaneously decreases. The volume expansion seems to be reflecting the increase of the covalent radii from the Co (126 pm) to Ru (146 pm)³⁰. Refinement of the diffraction patterns

TABLE I. Unit cell parameters and volume as obtained from the refinement of the X-ray powder diffraction patterns.

x	a (Å)	b (Å)	c (Å)	V (Å ³)
0.10	6.8344	4.2188	7.2717	209.6671
0.20	6.8216	4.2267	7.3048	210.6173
0.21	6.8204	4.2261	7.3026	210.4879
0.22	6.8189	4.2279	7.3079	210.6840
0.23	6.8178	4.2272	7.3085	210.6325
0.24	6.8131	4.2280	7.3145	210.6999
0.25	6.8150	4.2320	7.3229	211.2003
0.26	6.8269	4.2385	7.3347	212.2355
0.27	6.8203	4.2363	7.3314	211.8247
0.28	6.8205	4.2390	7.3392	212.1890
0.29	6.8133	4.2373	7.3389	211.8711
0.30	6.8077	4.2373	7.3413	211.7662
0.40	6.7880	4.2454	7.3704	212.3984
0.50	6.7709	4.2577	7.4046	213.4669
0.60	6.7522	4.2710	7.4416	214.6050
0.70	6.7336	4.2868	7.4741	215.7451
0.80	6.7137	4.3015	7.5041	216.7105
0.90	6.6909	4.3212	7.5290	217.6849

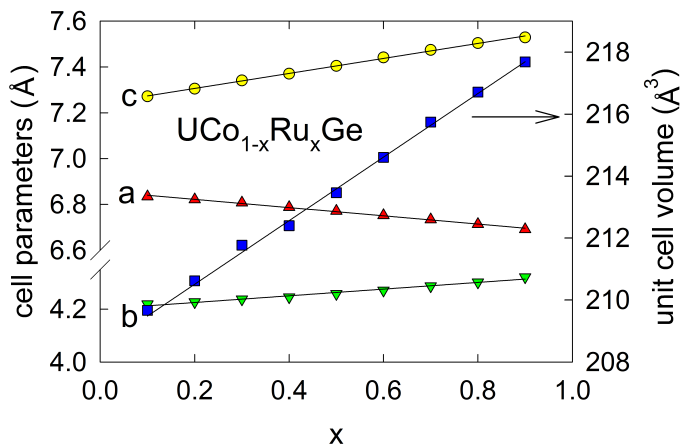


FIG. 2. (Color online) - Concentration dependence of the lattice parameters and unit cell volume in $\text{UCo}_{1-x}\text{Ru}_x\text{Ge}$ system. The lines serve as guides for the eye.

showed, that the Ru atoms really substitute only Co atoms on their sites. If we implemented the site $\text{Co}(\text{Ru})\text{-Ge}$ mixing the resulting R factor of such fit was always worse.

The XRPD patterns also allowed us to plot evolution of the $d_{\text{U-U}}$ distance. Although the unit cell volume expands towards Ru the $d_{\text{U-U}}$ distance contracts (see Fig. 3). It is not surprising result considering that the shortest $d_{\text{U-U}}$ is along the crystallographic axis a . It is only the one which contracts with the increasing Ru content.

We have performed series of the magnetization and AC susceptibility measurements on samples over a wide Ru doping range. In low Ru concentrations T_C steeply

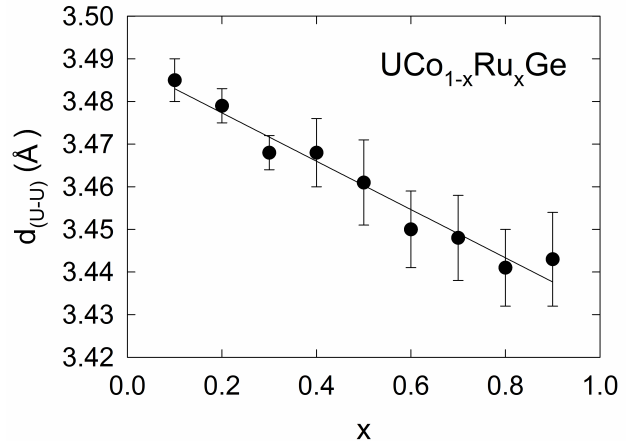


FIG. 3. Evaluated $d_{\text{U-U}}$ distances from the XRPD patterns. The $d_{\text{U-U}}$ interatomic distance evidently shortens with increasing Ru content.

increases with increasing x in agreement with results presented in previous work¹⁵. This trend terminates at $x_{\text{max}} \approx 0.1$ where the ordering temperature reaches its maximum $T_{C,\text{max}} \approx 8.6$ K, which is almost three times higher in comparison to the $T_C = 3$ K of the parent compound³ and it compares to the value found by Huang et al. in the case of Fe doping¹⁹. Further increase of the substituted Ru atoms on the Co site yields steady suppression of the ferromagnetic phase when the T_C drops to zero near critical concentration $x_{cr} \approx 0.3$ (see Fig. 12). The concentration evolution of T_C trend is followed by simultaneous development of the spontaneous moment. The magnetization curves clearly show rapid increase of the spontaneous moment up to $\sim 0.1 \mu_B/\text{f.u.}$ for $x \approx 0.1$ which is followed by a steady decrease with further increasing x . We have estimated the spontaneous magnetic moment μ_{spont} from the magnetization curves $M(H)$ measured at 1.85 K by extrapolating the magnetic moment from the high magnetic fields to zero (see Fig. 4). The values of the spontaneous moments determined for all samples are listed in the Table II and plotted in the complex phase diagram in Fig. 12.

The T_C values were determined from the Arrott plot³¹. For this purpose we have measured magnetization curves up to the 7 T at various temperatures around expected T_C for each sample. The Arrott plots were strongly non-linear in our case. Therefore we tried to evaluate the curves by the third degree polynomial function (see modeling example in Fig. 5) in order to find the interception with the M^2 axis of the plot. Extrapolation of the cross-sections with M^2 axis for the different temperatures to the value for $M^2 = 0$ was figured out as an estimation of the final T_C . Example of this construction is in the inset of Fig. 5.

We certainly tried to understand the nonlinearity of the Arrott plots. Cubic dependence in the M^2 vs H/M clearly suggests presence of a component linearly field

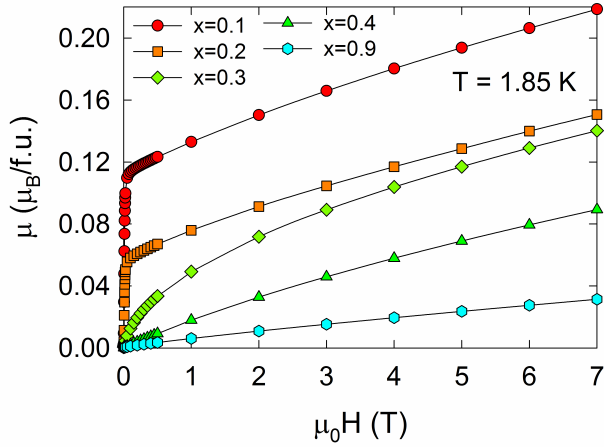


FIG. 4. (Color online) - Magnetization curves measured at $T = 1.85$ K for different concentrations of Ru up to the 7 T. Only representative concentrations are plotted for clarity.

TABLE II. Values of the spontaneous magnetic moment μ_{spont} , T_C from Arrott plot construction, from AC susceptibility, from magnetization data, specific heat and Sommerfeld gamma coefficient as determined for various concentration of Ru.

x	μ_{spont} (μ_B)	$T_{C,\text{Arrott}}$ (K)	$T_{C,\text{AC}}$ (K)	$T_{C,\text{mag}}$ (K)	$T_{C,\text{Cp}}$ (K)	γ ($\frac{\text{mJ}}{\text{mol}\cdot\text{K}^2}$)
0	0.0300	-	-	2.50	-	-
0.01	0.0330	4.20	-	4.00	-	-
0.05	0.0750	8.30	-	7.50	-	-
0.10	0.1060	8.62	-	8.20	8.60	0.0861
0.20	0.0540	5.70	-	5.40	5.70	0.1066
0.21	0.0580	5.70	5.20	5.40	5.90	0.1100
0.22	0.0594	5.01	4.70	5.00	5.30	0.1133
0.23	0.0568	4.68	4.20	4.60	4.30	0.1152
0.24	0.0270	3.55	3.50	3.60	3.80	0.1258
0.25	0.0300	3.49	3.40	3.40	3.30	0.1333
0.26	0.0213	2.51	2.80	2.80	3.00	0.1353
0.27	0.0223	2.77	2.40	2.60	2.80	0.1435
0.28	0.0219	2.32	1.90	2.30	2.70	0.1405
0.29	0.0077	-	1.44	-	1.40	0.1529
0.30	0.0013	-	-	-	-	0.1598
0.40	0.0011	-	-	-	-	0.1523
0.50	0.0001	-	-	-	-	0.1490

dependent to the magnetization. As an evidence for this scenario stands the strong magnetic uniaxiality of the system with the c axis as the easy magnetization direction²¹. Contribution of the hard axes (a and b) to the field dependence of the magnetization is linear (i.e. paramagnetic). For this purpose we tried to subtract the linear term from our measured magnetization M obtaining the corrected value $M^* = M - a \cdot H$. We have obtained linear isotherms for the value of the slope $a = 0.006$ in the revised Arrott plot construction. Example of this data treatment is presented on the exemplary case of the $\text{UCo}_{0.77}\text{Ru}_{0.23}\text{Ge}$ in Fig. 6.

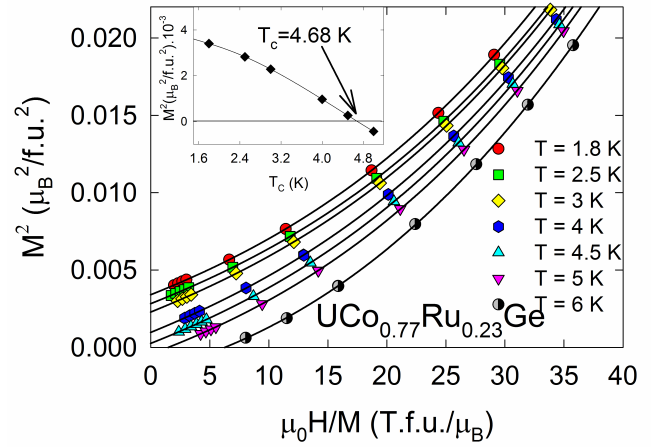


FIG. 5. (Color online) - Arrott plot constructed for the estimation of the T_C . Example is given for the $\text{UCo}_{0.77}\text{Ru}_{0.23}\text{Ge}$ compound. Solid lines are the third order polynomial functions. The inset shows that the T_C is taken as a value for which the intersection with the M^2 axis would be zero.

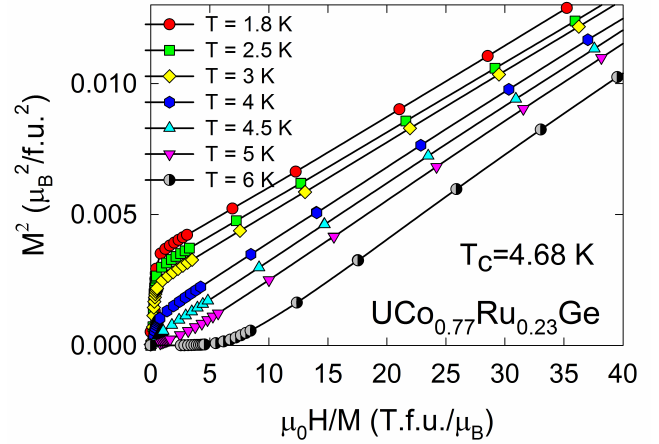


FIG. 6. (Color online) - Revised Arrott plot after subtraction of the linear term with the slope $a = 0.006$ from the magnetization data measured on the $\text{UCo}_{0.77}\text{Ru}_{0.23}\text{Ge}$ sample.

Temperature dependence of the magnetization follows results from the magnetization curves (see Fig. 7). Development of the spontaneous and saturated magnetic moment is also observable on the change of the shape of magnetization curves (see Fig. 4).

The values of ordering temperatures obtained from the Arrott plot analysis are in good agreement with the position of the inflection points in the $M(T)$ dependencies (measured in the external field of 10 mT) and also with the maxima of the real parts of the AC susceptibility χ'

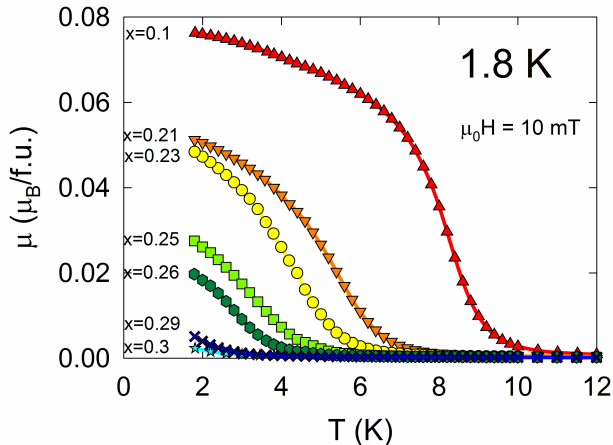


FIG. 7. (Color online) - Temperature dependence of magnetization for different concentrations of Ru measured in external magnetic field of 10 mT. Drop of T_C and spontaneous magnetic moment is evident with increased Ru content.

(see Fig. 8). This observation allowed us to estimate T_C also in the temperature region of 350 mK – 1.8 K where we could use a home-made coil for the low temperature AC susceptibility measurements³² (sample with $x = 0.29$ in Fig. 8). The low temperature AC susceptibility for sample $x = 0.29$ still revealed well developed peak at 1.4 K signaling FM order. No sign of any anomaly was detected for $x = 0.31$ down to the temperature 350 mK which seems to be the terminal concentration of the Ru for ferromagnetism existence in the $\text{UCo}_{1-x}\text{Ru}_x\text{Ge}$ system.

Temperature dependences of the specific heat $C_p(T)$ at low temperatures support our results from the magnetization measurements. We have used the inflection point of the C_p/T vs. T anomaly as an estimation of the Curie temperatures T_C due to rather broad transitions for $0.1 < x < 0.3$. These values are comparable to those derived from magnetization data. These T_C values are also plotted in the Fig. 12. We subsequently subtracted the lattice contribution using the fit of the lattice specific heat as a $C_{\text{lat}}(T) = \beta T^3$. We have typically received the values of the $\beta \approx (0.52 - 0.56) \cdot 10^{-3} \text{ J} \cdot \text{mol}^{-1} \text{ K}^{-4}$ i.e. Debye temperature of 151 – 155 K was evaluated for each sample in the temperature interval between T_C and 20 K. Figure 9 shows f -electron specific heat $C_m = C - C_{\text{lat}}$ plotted as C_m/T vs $\log T$. The anomaly at T_C is clearly smeared down and shifted to lower temperatures with increasing of the Ru concentration. Finally, the specific heat shows sign of almost linear trend in the temperature region (1 – 10 K) for $x \approx 0.31$. We will discuss later this behavior in scenario of the nFL state development. nFL is characterized by the logarithmic dependence of the specific heat divided by temperature $C_m(T)/T = c \ln(T_0/T)$ ^{33,34}. This is expected for the concentrations in the vicinity of a QCP.

However, our data do not follow linear prediction in the whole temperature range. Nevertheless it is

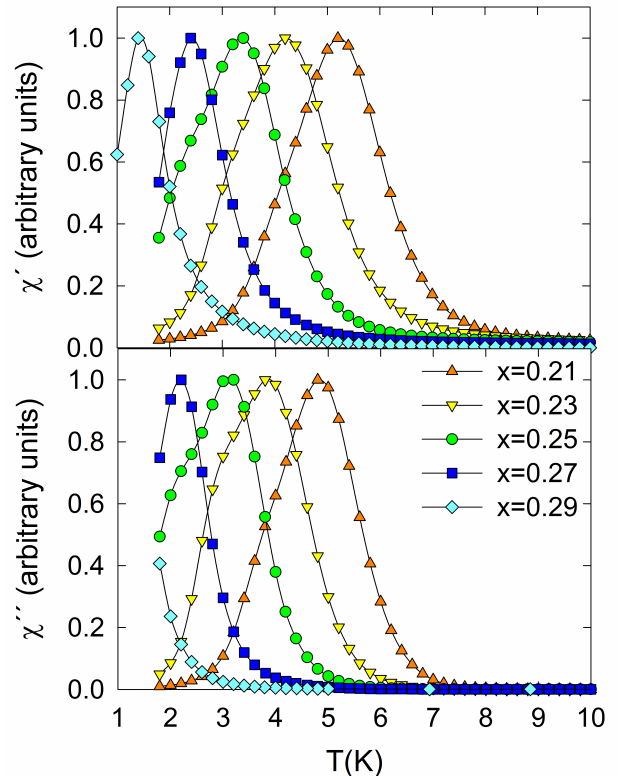


FIG. 8. (Color online) - Real (χ') and imaginary (χ'') part of the AC susceptibility. Data are plotted in the arbitrary units and normalized because the home made coil for measurement in ^3He (used for $x = 0.29$) allows only the relative measurement. Some datasets are hidden for clarity of the figure.

very similar to the case of the $\text{UCo}_{1-x}\text{Fe}_x\text{Ge}$ system¹⁹ which is claimed as exhibiting nFL behavior. Contrary to the $\text{UCo}_{1-x}\text{Fe}_x\text{Ge}$ system¹⁹ a perfectly linear trend was found around critical concentration in the similar $\text{URh}_{1-x}\text{Ru}_x\text{Ge}$ system¹⁸. Origin of this effect will be discussed later.

If we calculate magnetic entropy S_{mag} integrated over the temperature range from 0.7 K up to the T_C for each sample we can observe steady decrease of this value from 0.13 R ln 2 for $x = 0.1$ down to the 0.006 R ln 2 at $x = 0.30$ (see Fig. 12) which is consistent with gradually disappearing itinerant magnetic moment when approaching QCP ($x \approx 0.31$). As the system approaches the critical concentration we can also observe dramatic increase of the Sommerfeld γ coefficient ($\gamma \sim x^2$) from the former 57 mJ/mol · K² (Ref.³⁵) for the parent UCoGe up to the 160 mJ/mol · K² at $x = 0.3$ near x_{cr} which is followed by decrease of the γ -value with increasing Ru concentration beyond x_{cr} . According to the prediction for the dependence of Curie temperature (T_C) on the value of con-

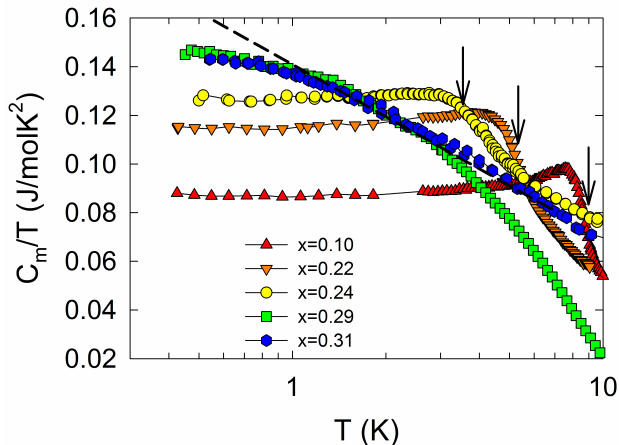


FIG. 9. (Color online) - Electron specific heat divided by temperature for samples with different Ru content in the logarithmic scale. Only few concentrations are plotted for clarity. Black arrows shows the position of T_C for the $x = 0.10$ and $x = 0.22$ at the inflection point. Dashed line shows linear dependence of the specific heat for $x = 0.31$.

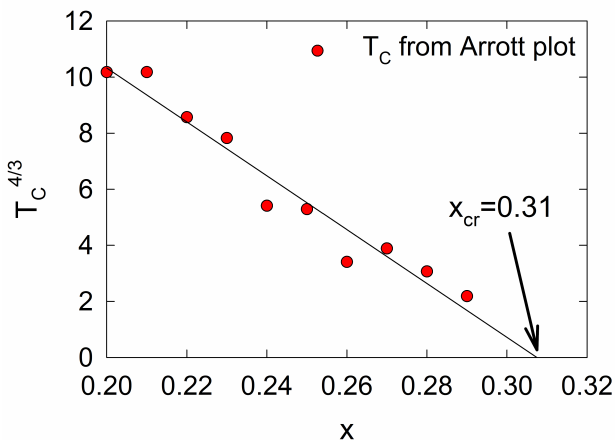


FIG. 10. (Color online) - Estimation of the critical concentration using the T_C from the Arrott plots as the most plausible values were used for construction of the picture. Linear behavior of the T_C support correctness to use the $T_C \sim (x_{cr} - x)^{3/4}$ law.

control parameter (x) for nFL ferromagnets by Millis and Hertz^{33,34} we are able to estimate the value of the critical concentration x_{cr} . The ordering temperature should obey $T_C \sim (x_{cr} - x)^{3/4}$. If we plot Curie temperatures in the region of $x = 0.2 - 0.3$ as a $T_C^{4/3} \sim x$ plot we should receive obvious linear behavior. A linear fit gives the estimation for the critical concentration as $x_{cr} \approx 0.31$. The fitted curve is included to the phase diagram in Fig. 12 and also displayed in detail in the separate Fig. 10.

The high temperature part of the temperature dependence of the electrical resistivity for all measured poly-

crystalline samples shows an initial increase up to the maximum at T_0 (see inset of the Fig. 11). An analogous effect is observed in the resistivity data measured on the UCoGe single crystal for current along the c -axis²¹. This resistivity increase effect is most likely connected with the spin fluctuations when $T^{5/3}$ spin fluctuation theory for a weak itinerant ferromagnet is applicable at temperatures below the knee²¹. The maximum can also well correspond with the field induced moment polarizability reported by Knafo et al.³⁶. Our data measured on polycrystalline samples reveal general increasing dependence of the temperature T_0 on the Ru content x but with no sign of a perfectly regular trend, which can be caused by polycrystalline materials. The reduced size of the effect measured on polycrystals is probably due to averaging the anisotropic resistivity. Even small sign of preferred orientation of grains in the polycrystal or its texture can dramatically change the temperature dependence of the measured electrical resistivity. Some samples exhibited well pronounced maximum at T_0 while the others showed rather broad plateau or even almost a common metallic features. The first case shows preferred orientation along the magnetic easy axis c while the broad plateau can be sign to the orientation along one of the hard magnetization axes (a or b). Nevertheless the overall increase of the T_0 corresponds to the fact that the knee is not present in the data measured on the polycrystalline samples up to the 300 K for the URuGe compound³⁷. The resulting temperature dependencies of the electrical resistivity ratios for selected polycrystalline samples are plotted in Fig. 11.

Anomalies connected with the transitions from ferromagnetic to the paramagnetic state are not so clearly visible on the polycrystalline data. Arrows in Fig. 11 show T_C obtained from the analysis of the Arrott plots. T_C estimated from the specific heat data are used for the samples with lower T_C in Fig. 11. It is obvious, that increased Ru content dramatically changes the curvature of the low temperature part of the resistivity in the UCo_{1-x}Ru_xGe system. We have performed fitting of the resistivity data taking into account contribution of the ferromagnetic magnon gap^{38,39} which was successfully used for evaluation of the resistivity data of the strongly anisotropic systems⁴⁰. For this reason we used equation (1)

$$\rho = \rho_0 + AT^2 + C_m T \Delta \left(1 + \frac{2T}{\Delta} \right) \exp \left(-\frac{\Delta}{T} \right) \quad (1)$$

The size of the gap varies in the interval $\Delta \approx 0.5 - 5$ K. We have employed the general expression $\rho = \rho_0 + AT^n$ for temperatures above T_C . The inflection point was used as an upper limit for the fitting because it is always presented in measured data, due to the increasing resistivity as it approaches maximum value at T_0 . The exponent gradually decreases as the Ru content approaches the critical concentration x_{cr} . The minimum value of $n \approx 1.13$ for $x = 0.31$ is close to the proposed linear tem-

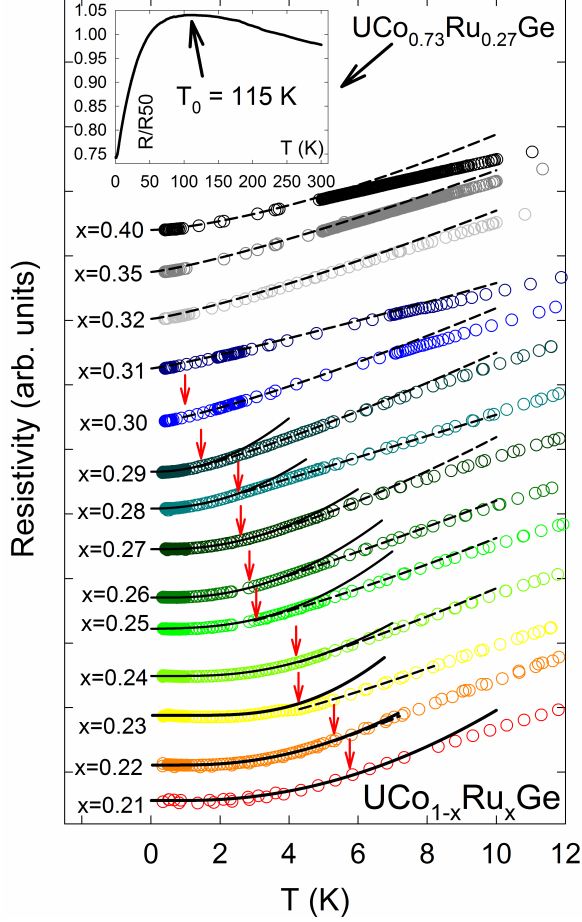


FIG. 11. (Color online) - Temperature dependence of the electrical resistivity for selected polycrystalline samples with gradual Ru content. Red arrows denote the T_C obtained from the Arrott plots analysis and from the heat capacity data. Solid lines are fitted by the Eq. (1). Dashed lines are fits to the $\rho = \rho_0 + AT^n$ equation. All curves are arbitrary horizontally shifted for better clarity. The inset shows one typical temperature dependence of the resistivity in the broad temperature range - $\text{UCo}_{0.73}\text{Ru}_{0.27}\text{Ge}$ compound was chosen as an example.

perature dependence of the resistivity according to the Millis and Hertz^{33,34} theory for nFL behavior in the 3D ferromagnet. The samples with higher concentration of the Ru ($x > x_{\text{cr}}$) exhibited steady recovery to the FL state pronounced as an increase of the value of n exponent. Results of the $\rho = \rho_0 + AT^n$ fits are plotted in the Fig. 11 and development of the exponent n is summarized in the $T - x$ phase diagram (Fig. 12). We have also observed quite low RRR ≈ 1.1 of the samples, given as a $\rho_{300\text{K}}/\rho_{0.4\text{K}}$, through the whole series of polycrystalline samples with $x > 0.2$. It shows that the chemical doping induces remarkable disorder in the system (see Fig. 12). We have found common value of the RRR for polycrystalline samples of parent UCoGe between 6 and 10. We calculated the logarithmic derivative of the electrical re-

sistivity according to the Eq. (2) in order to see direct change of the n exponent as a function of temperature

$$n = \frac{d \ln(\rho - \rho_0)}{d \ln T} \quad (2)$$

The results of this analysis are plotted in the phase diagram (Fig. 12). It reveals a significant change of the exponent in the ordered region where $n \geq 2$ and in the higher temperatures where $n < 2$. Remarkable is a sharp drop of the n value near the critical concentration down to the lowest temperatures surrounded by regions of higher n (rapidly increasing on the FM side for $x < x_{\text{cr}}$ and slower increase on the paramagnetic side). Absence of the sharp transition at the T_C for polycrystalline samples leads to the broadened region of the $n \approx 2$ exponent also above the Curie temperature.

We have applied the first-principles theoretical methods to better understand the changes in the electronic structure of the $\text{UCo}_{1-x}\text{Ru}_x\text{Ge}$ system. While the density of states of the parent compound UCoGe is known (Ref.⁴¹) the information about the paramagnetic URuGe were missing. Calculated total and partial DOS of the URuGe are plotted in Fig. 13.

We used the calculated URuGe band structure to apply a simple model of Silva Neto et al.⁴² based on the periodic Anderson model^{43,44}. This simplified model proposes the key role of the $nd - 5f$ hybridization (V_{df}) in the non-monotonous evolution of T_C in the $\text{URh}_{1-x}\text{Co}_x\text{Ge}$ system. They described the T_C evolution as a consequence of the broadening of the nd and $5f$ bands (W_d, W_f) and mutual shift of their centers ($C_{Td} - C_{Uf}$) related as follows⁴²

$$V_{df} = \frac{W_d W_f}{C_{Td} - C_{Uf}} \quad (3)$$

If we follow this model for the $\text{UCo}_{1-x}\text{Ru}_x\text{Ge}$ system we can qualitatively describe the non-monotonous evolution of T_C . The concentration dependence of the nd band broadness is assumed to be linear following Eq. 4

$$W_d(x) = W_d^{Co}(1-x) + W_d^{Ru}(x) \quad (4)$$

where $W_d^{Co} = 6.1\text{eV}$ (Ref.⁴¹) and $W_d^{Ru} = 8.7\text{eV}$ (see Fig. 13) and $W_f = 0.43\text{eV}$ (Ref.⁴¹). Such behavior is consistent with other UTX ($T =$ transition metal, $X = p$ element) compounds where the d band broadens while we move from the $3d$ to the $4d$ transition metals⁴⁵. Consequently the $(C_{Td} - C_{Uf})(x) = \Delta C_{df}(x)$ deviates from the linearity

$$\Delta C_{df} = \Delta C_{df}^{Co}(1-x) + \Delta C_{df}^{Ru}x + \delta' x^2(1-x) + \delta'' x(1-x)^2 \quad (5)$$

We used the values from calculated DOSes, i.e. $\Delta C_{df}^{Ru} = 0.65\text{eV}$ and $\Delta C_{df}^{Co} = 1.5\text{eV}$ (Ref.⁴¹) and adjustable parameters were taken as $\delta' = 2 \cdot 10^{-5}$ and

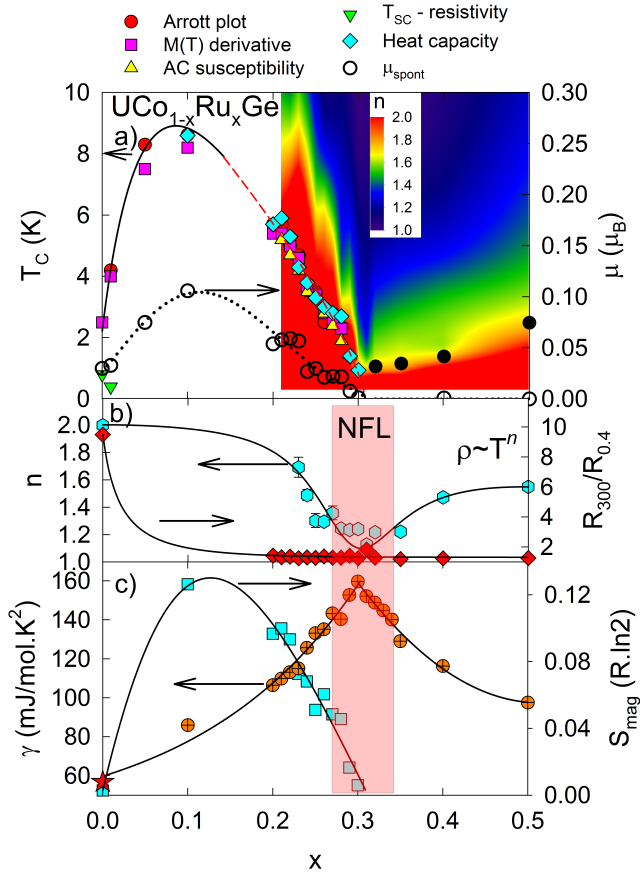


FIG. 12. (Color online) - Panel a) shows $T-x$ phase diagram based on measurements of polycrystalline samples. T_C s were estimated from the various methods mentioned in the text. Plot is supplemented by the results of the the electrical resistivity measurement revealing occurrence of superconductivity in the parent UCoGe compound and in the polycrystalline $\text{UCo}_{0.99}\text{Ru}_{0.01}\text{Ge}$ - this two data points are taken from Ref.¹⁵ (green triangle). Black solid line is only guide for the eye while the red dashed part is a fit of $T_C \sim (x_{\text{cr}} - x)^{3/4}$. Right axes shows development of the spontaneous magnetic moment (dashed line is only guide for the eye). Contour plot shows local exponent in the resistivity obtained as $n = \frac{d \ln(\rho - \rho_0)}{d \ln T}$. Black filled circles show temperature where resistivity starts to deviate from the T^2 dependence. Panel b) shows evolution of the coefficients n from the fitting of the low temperature dependence of the electrical resistivity with equation $\rho = \rho_0 + AT^n$ for $T > T_C$. Right axis shows $\text{RRR} = \rho_{300\text{K}}/\rho_{0.4\text{K}}$ as a function of x . Panel c) shows development of the Sommerfeld γ coefficient obtained from the $C_m(T)$ data and magnetic entropy S_{mag} (value for the parent UCoGe is taken from Ref.¹³ and is marked by star).

$\delta'' = 2$. Such approach gives us non-monotonous dependence of the $d-f$ hybridization term V_{df} starting with $V_{df}(x=0) \approx 1.73$ for UCoGe (in agreement with Ref.⁴²), $V_{df}(x=1) \approx 5.55$ for URuGe and $V_{df}(x \approx 0.3) \approx 1.9$ as estimated for the ferromagnetic QCP⁴². The overall $V_{df}(x)$ dependence starts with its decrease which causes enhancement of the density of f states at the Fermi

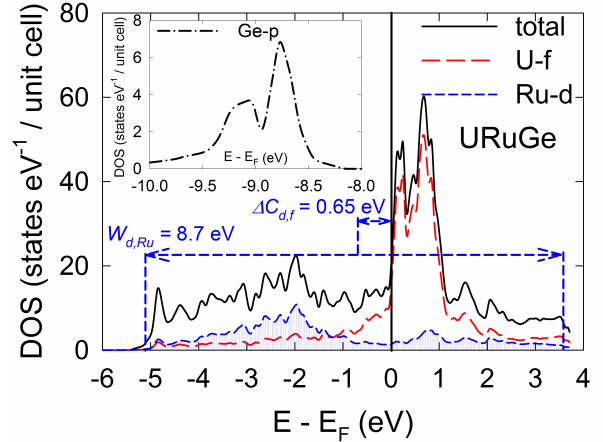


FIG. 13. (Color online) Total DOS and partial DOS for U f states and Ru d states. Width of the d -band ($W_{d,Ru}$) and its center $\Delta C_{d,f}$ are marked by dashed arrows. Inset shows contribution of the Ge p states far from the Fermi level.

level⁴⁶. Using usual approach for the itinerant ferromagnets we can estimate the ordering temperature as a function of the density of states at the Fermi level $T_C \sim (IN(E_F) - 1)^{3/4}$ where I is the so called Stoner integral⁴⁷. In this outlook we can attribute the initial increase of T_C to the enhanced $N(E_F)$. At $x \approx 0.07$ the $d-f$ hybridization reaches its minimum value $V_{df} = 1.7$ and starts to increase for increasing x . This point qualitatively agrees with the position of maximum T_C in experimental data at $x \approx 0.1$. As the concentration of the dopant is higher the d -band is shifted closer to the position of the f -band and the hybridization increases which is leading to the lowering of the f -DOS contribution to the density of states at the Fermi level⁴⁶. For the reason mentioned above the ordering temperature decreases and reaches zero near $x_{\text{cr}} \approx 0.3$.

IV. DISCUSSION

In general, magnetism of the uranium systems is strongly affected by the direct overlap of the $5f$ wave functions with subsequent delocalization of the $5f$ electron and consequent washout of the $5f$ magnetic moments. One would expect in the most simple model a continuous vanishing of the FM from UCoGe to URuGe due to the contraction of the d_{U-U} distance approaching Hill limit⁴⁸ (Fig. 3 and Fig. 14).

But it is not valid, not only in the $\text{UCo}_{1-x}\text{Ru}_x\text{Ge}$ system but also in many neighboring others like $\text{UCo}_{1-x}\text{Fe}_x\text{Ge}$ ¹⁹, $\text{URh}_{1-x}\text{Ru}_x\text{Ge}$ ¹⁸ or $\text{URh}_{1-x}\text{Co}_x\text{Ge}$ ¹⁷. The situation is more complex and $5f$ -ligand hybridization should be taken into account. The significant influence of the hybridization is apparent in non-monotonous development of the critical temperatures in UTGe com-

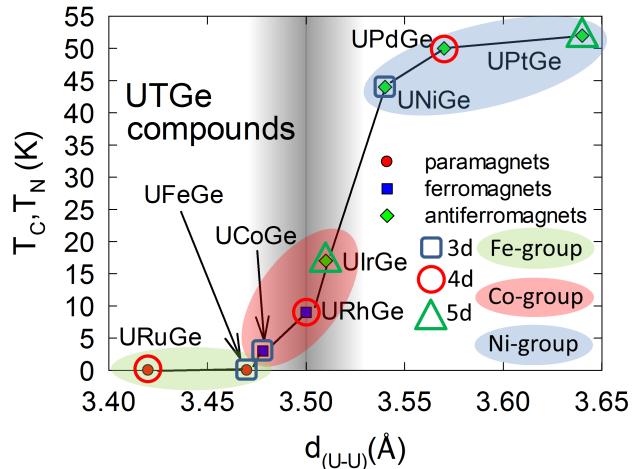


FIG. 14. (Color online) - Illustrative plot showing dependence of the ordering temperature of the $UTGe$ compounds ($T =$ transition metal) on the shortest distance between two nearest uranium atoms (d_{U-U}). Shaded region spreads around Hill limit (3.5 \AA)⁴⁸ valid for uranium. Position of the $UFeGe$ is exceptional because the $UFeGe$ does not keep the $TiNiSi$ -type structure²⁵. Information about the structure and magnetic features of the $UOsGe$ compound is missing till today to complete and confirm the suggested trends.

pounds when one moves from $3d$ to $5d$ or from the Fe-group to Ni-group. Thus, the explanation of the non-monotonous (dome-like) concentration dependence of the Curie temperature and ferromagnetic state seems to be controlled by the $5f(U) - nd(T)$ hybridization which apparently plays dominant role in these materials. The hybridization plays a dual role in magnetism: a) it can mediate an indirect exchange interaction which is promoting magnetic ordering, b) it disturbs the atomic character of the involved electron wave-functions which leads to delocalization of the $5f$ electron and washing out the $5f$ -magnetic moments.

Within this scenario we have followed the simple model dealing with the widths and positions of the nd and $5f$ bands described in Ref.⁴² to identify mechanism responsible for the FM behavior in $UCo_{1-x}Ru_xGe$. The dome-like character of the phase diagram in the case of isoelectronic substitution in the system $URh_{1-x}Co_xGe$ results from the competition between the reduction of the $d-f$ hybridization caused by narrowing of the d band. Co $3d$ band character and simultaneous approaching of the d band towards the f band lead to the enhancement of the hybridization⁴². Our non-isoelectronic substitution in $UCoGe$ of Co by Ru causes broadening of the d band from $3d$ to the $4d$ transition metal-like. Together with the mutual shift of the d and f bands towards them itself we can qualitatively describe dome-like dependence of the ordering temperature T_C . $UCo_{1-x}Ru_xGe$ system is important

confirmation of the trend. Changes in the $f-d$ hybridization varies magnetic ground state also in the analogous systems like $URh_{1-x}Ru_xGe$ ¹⁸ and $UCo_{1-x}Fe_xGe$ ¹⁹.

The magnitude of the hybridization is well reflected in relation to the $ZrNiAl$ -type $UTAl$ compounds ($T =$ transition metal), which can also originate in the different geometry of the ions. The $UFeAl$ ⁴⁹ and $URuAl$ ⁵⁰ are also paramagnets, $UCoAl$ ⁵¹ compound is close to a ferromagnetic instability and the $URhAl$ ⁵⁰ one is a strong ferromagnet. Ferromagnetic domes also develop in the $URh_{1-x}Ru_xAl$ ⁵², $UCo_{1-x}Ru_xAl$ ⁵³ and $URh_{1-x}Ru_xGa$ ⁵². However the T_C s are significantly higher and the domes survive up to much higher concentrations of the nonmagnetic analogue. In the $UCo_{1-x}Ru_xAl$ ⁵³ almost up to the nonmagnetic $URuAl$ compound. It is evident that the $d-f$ hybridization in the alloying $TiNiSi$ -type $UTGe$ compounds works rather as the delocalization mechanism of the $5f$ electrons while in the $ZrNiAl$ -type $UTAl$ compounds as the indirect interaction mediating stable magnetic order. Strong delocalization of the $5f$ electrons is reflected by strong decrease of the magnetic entropy S_{mag} down to the $0.006 R \ln 2$ for $x \approx 0.3$ points on the itinerant nature of the weak magnetism in the vicinity of the critical concentration. We would expect magnetic entropy equal to zero⁵⁴ for an ideal itinerant ferromagnet.

We cannot also neglect the influence of the contraction of the d_{U-U} distance. The original increase of the T_C at the low Ru concentration contradicts the d_{U-U} behavior and $5f-d$ hybridization seems to be the leading effect responsible for the ferromagnetism behavior. The d_{U-U} interatomic distance can partly contribute to later development of the nFL and paramagnetic state in the higher concentration of the Ru because the pure compounds in $AnTGe$ ($An =$ actinide element, $T =$ transition metal) series surprisingly fulfill the Hill behavior as was suggested in the phase diagram in Ref⁵⁵. However, the ratio and separation of the hybridization effect from the influence of the d_{U-U} cannot be carried out on the basis of our available macroscopic data.

Our results of the temperature dependence of the electrical resistivity and heat capacity show signs of the nFL behavior in the vicinity of x_{cr} pointing on the possible presence of the FM QCP. We have observed drop of the n exponent in the temperature dependence of resistivity ($\rho = \rho_0 + AT^n$) and almost linear dependence of the reduced heat capacity $C_m(T)/T = c \ln(T_0/T)$ at low temperatures what would be in agreement with the theoretical predictions of Millis and Hertz^{33,34}. Another evidence for the FM QCP is rapid increase of the Sommerfeld coefficient γ near x_{cr} . The proposed scenario is also sustained by scaling of the ordering temperature with control parameter itself; obeying $T_C \sim (x_{cr} - x)^{3/4}$ and giving estimation of critical concentration $x_{cr} \approx 0.31$. Our heat capacity data follow the $C_m(T)/T = c \ln(T_0/T)$ function only in very limited region in our system in the lowest temperatures. Nevertheless, the same effect was observed weakly in the case of $URh_{1-x}Ru_xGe$ ¹⁸ and in the $UCo_{1-x}Fe_xGe$ ¹⁹ compounds. However, in our

UCo_{1-x}Ru_xGe compound is this effect the strongest. We suppose that the effect originates from non-isoelectronic doping and mixture of the 3*d*-4*d* bands which can cause that the nFL state is not so well developed because of the disorder effect.

Thus, we conclude that the tuning of the system to the QCP by doping brings large obstruction in the form of disorder. This effect can be neglected in the case of pressure or magnetic field driven QPT, but in our case it deserves deeper discussion. Disorder caused by doping can be one of the reasons of the lacking of SC in the proximity of these secondary QCPs including our UCo_{1-x}Ru_xGe system. While SC in the UCoGe is proposed to be unconventional³ it should be very sensitive to the impurities according to the generalized form of the Abrikosov-Gor'kov pair-breaking theory^{56,57}. Our phase diagram in Fig. 12 is supplemented by two data points from Ref.¹⁵ showing how rapidly is SC lost within the system. Iron doping brings comparable results¹⁹, while external pressure keeps SC almost untouched in wide pressure range⁵⁸. Disorder can also in some cases emulate nFL behavior⁵⁹, so interpretation of such results should always be done with the proper precaution. The effect of disorder can in principle also affect the order of the phase transition, i.e. blurring the first-order transition to the continuous second-order one. Our samples showed rather small RRR values ~ 1.2 which is similar to the compounds UCo_{1-x}Fe_xGe¹⁹, URh_{1-x}Ru_xGe¹⁸ where transition to the FM state is proposed to be of the second-order, as well.

V. CONCLUSIONS

We have successfully prepared series of the polycrystalline samples of UCoGe doped by Ru in the wide con-

centration range. Ru doping leads to developments of the FM dome between $x = 0 - 0.31$ when maximum of the $T_C = 8.6$ K and spontaneous moment of $\mu_{\text{eff}} = 0.1 \mu\text{B}$ appears at the $x \approx 0.1$. Further increase of the Ru content up to the $x = 0.31$ leads to the vanishing of the FM and critical exponents behavior points to the merging of the nFL state. The nFL state is strongly influenced by disorder of the system because of the non-isoelectronic mixture of the 3*d* and 4*d* bands. The band structure analysis assigns the evolution of ferromagnetism to the effects of the 5*f*-ligand hybridization. Our work also confirmed that the UCoGe compound represents a unique example of the system in the vicinity of the FM instability connected with evolution of the the nFL state. That nFL state can again develop in the neighboring doped systems. Further study of the region around the critical concentration including the measurements under the external pressure performed on single crystals is envisaged to deeply understand the background of the proposed nFL state.

ACKNOWLEDGMENTS

This work was supported by the Czech Science Foundation no. P204/12/P418 and the Charles University in Prague, project GA UK No.720214. Experiments performed in MLTL (see: <http://mltl.eu/>) were supported within the program of Czech Research Infrastructures (project LM2011025).

* michal.valiska@gmail.com

¹ A. Huxley, I. Sheikin, E. Ressouche, N. Kernavanois, D. Braithwaite, R. Calemczuk, and J. Flouquet, *Physical Review B* **63**, 144519 (2001).
² D. Aoki, A. Huxley, E. Ressouche, D. Braithwaite, J. Flouquet, J.-P. Brison, E. Lhotel, and C. Paulsen, *Nature* **413**, 613 (2001).
³ N. T. Huy, A. Gasparini, D. E. de Nijs, Y. Huang, J. C. P. Klaasse, T. Gortenmulder, A. de Visser, A. Hamann, T. Gorklach, and H. von Lohneysen, *Physical Review Letters* **99**, 067006 (2007).
⁴ C. Pfleiderer, S. R. Julian, and G. G. Lonzarich, *Nature* **414**, 427 (2001), 10.1038/35106527.
⁵ D. v. d. Marel, H. J. A. Molegraaf, J. Zaanen, Z. Nussinov, F. Carbone, A. Damascelli, H. Eisaki, M. Greven, P. H. Kes, and M. Li, *Nature* **425**, 271 (2003).
⁶ C. Pfleiderer, G. J. McMullan, S. R. Julian, and G. G. Lonzarich, *Physical Review B* **55**, 8330 (1997).
⁷ A. Schroder, G. Aeppli, R. Coldea, M. Adams, O. Stockert, H. v. Lohneysen, E. Bucher, R. Ramazashvili, and

P. Coleman, *Nature* **407**, 351 (2000).

⁸ H. v. Lohneysen, T. Pietrus, G. Portisch, H. G. Schlager, A. Schroder, M. Sieck, and T. Trappmann, *Physical Review Letters* **72**, 3262 (1994).
⁹ J. Custers, P. Gegenwart, H. Wilhelm, K. Neumaier, Y. Tokiwa, O. Trovarelli, C. Geibel, F. Steglich, C. Pepin, and P. Coleman, *Nature* **424**, 524 (2003).
¹⁰ C. Pfleiderer and A. D. Huxley, *Physical Review Letters* **89**, 147005 (2002).
¹¹ C. Pfleiderer, *Journal of Physics: Condensed Matter* **17**, S987 (2005).
¹² D. Aoki and J. Flouquet, *Journal of the Physical Society of Japan* **81**, 011003 (2012).
¹³ A. Gasparini, Y. K. Huang, J. Hartbaum, H. von Lohneysen, and A. de Visser, *Physical Review B* **82**, 052502 (2010).
¹⁴ D. Aoki, T. D. Matsuda, V. Taufour, E. Hassinger, G. Knebel, and J. Flouquet, *Journal of the Physical Society of Japan* **78**, 113709 (2009).

- ¹⁵ J. Pospisil, J. P. Vejpravova, M. Divis, and V. Sechovsky, *Journal of Applied Physics* **105**, 07E114 (2009).
- ¹⁶ R. Troc and V. H. Tran, *Journal of Magnetism and Magnetic Materials* **73**, 389 (1988).
- ¹⁷ N. T. Huy and A. de Visser, *Solid State Communications* **149**, 703 (2009).
- ¹⁸ N. T. Huy, A. Gasparini, J. C. P. Klaasse, A. de Visser, S. Sakarya, and N. H. van Dijk, *Physical Review B* **75**, 212405 (2007).
- ¹⁹ K. Huang, J. J. Hamlin, R. E. Baumbach, M. Janoschek, N. Kanchanavatee, D. A. Zocco, F. Ronning, and M. B. Maple, *Physical Review B* **87**, 054513 (2013).
- ²⁰ N. T. Huy, D. E. de Nijs, A. Gasparini, J. C. P. Klaasse, A. de Visser, and N. H. van Dijk, *Physica B: Condensed Matter* **403**, 1260 (2008).
- ²¹ J. Pospisil, K. Prokes, M. Reehuis, M. Tovar, J. Poltieroja Vejpravova, J. Prokleska, and V. Sechovsky, *Journal of the Physical Society of Japan* **80**, 084709 (2011).
- ²² H. Rietveld, *Journal of Applied Crystallography* **2**, 65 (1969).
- ²³ J. Rodriguez-Carvajal, *Physica B: Condensed Matter* **192**, 55 (1993).
- ²⁴ T. Roisnel and J. Rodriguez-Carvajal, in *EPDIC 7 - Seventh European Powder Diffraction Conference*, edited by R. Delhez and E. Mittemeijer (Trans Tech Publications).
- ²⁵ F. Canepa, P. Manfrinetti, M. Pani, and A. Palenzona, *Journal of Alloys and Compounds* **234**, 225 (1996).
- ²⁶ J. P. Perdew and Y. Wang, *Physical Review B* **45**, 13244 (1992).
- ²⁷ J. P. Perdew, K. Burke, and M. Ernzerhof, *Physical Review Letters* **77**, 3865 (1996).
- ²⁸ K. Schwarz, P. Blaha, and G. K. H. Madsen, *Computer Physics Communications* **147**, 71 (2002).
- ²⁹ L. Vegard, *Zeitschrift fur Physik A Hadrons and Nuclei* **5**, 17 (1921).
- ³⁰ B. Cordero, V. Gomez, A. E. Platero-Prats, M. Reves, J. Echeverria, E. Cremades, F. Barragan, and S. Alvarez, *Dalton Transactions* **0**, 2832 (2008).
- ³¹ A. Arrott, *Physical Review* **108**, 1394 (1957).
- ³² J. Prokleska, J. Pospisil, J. Vejpravova Poltieroja, V. Sechovsky, and J. Sebek, *Journal of Physics: Conference Series* **200**, 012161 (2010).
- ³³ A. J. Millis, *Physical Review B* **48**, 7183 (1993).
- ³⁴ J. A. Hertz, *Physical Review B* **14**, 1165 (1976).
- ³⁵ A. Gasparini, Y. K. Huang, N. T. Huy, J. C. P. Klaasse, T. Naka, E. Slooten, and A. de Visser, *Journal of Low Temperature Physics* **161**, 134 (2010).
- ³⁶ W. Knafo, T. D. Matsuda, D. Aoki, F. Hardy, G. W. Scheerer, G. Ballon, M. Nardone, A. Zitouni, C. Meingast, and J. Flouquet, *Physical Review B* **86**, 184416 (2012).
- ³⁷ V. H. Tran, R. Troc, and D. Urski, *Journal of Magnetism and Magnetic Materials* **87**, 291 (1990).
- ³⁸ N. H. Andersen and H. Smith, *Physical Review B* **19**, 384 (1979).
- ³⁹ N. H. Andersen, "Electrical resistivity investigations on metallic rare-earths," in *Crystalline Electric Field and Structural Effects in f-Electron Systems* (Springer US, 1980) Chap. 41, pp. 373–387.
- ⁴⁰ K. Uhlirova, M. Divis, J. Pospisil, S. Danis, and V. Sechovsky, *Journal of the Physical Society of Japan* **81**, 094703 (2012).
- ⁴¹ M. Divis, *Physica B-Condensed Matter* **403**, 2505 (2008).
- ⁴² M. B. S. Neto, A. H. C. Neto, J. S. Kim, and G. R. Stewart, *Journal of Physics: Condensed Matter* **25**, 025601 (2013).
- ⁴³ C. D. Batista, J. Bonca, and J. E. Gubernatis, *Physical Review Letters* **88**, 187203 (2002).
- ⁴⁴ C. D. Batista, J. Bonca, and J. E. Gubernatis, *Physical Review B* **68**, 214430 (2003).
- ⁴⁵ T. Gasche, M. S. S. Brooks, and B. Johansson, *Journal of Physics: Condensed Matter* **7**, 9499 (1995).
- ⁴⁶ D. M. Newns and N. Read, *Advances in Physics* **36**, 799 (1987).
- ⁴⁷ T. Moriya, *Spin Fluctuations in Itinerant Electron Magnetism* (Springer Berlin Heidelberg, 2012).
- ⁴⁸ H. H. Hill, pp. 1 – 19.
- ⁴⁹ R. Troc, V. H. Tran, F. G. Vagizov, and H. Drulis, *Journal of Alloys and Compounds* **200**, 37 (1993).
- ⁵⁰ A. Veenhuizen, P., R. de Boer, F., A. Menovsky, A., V. Sechovsky, and L. Havela, *J. Phys. Colloques* **49**, C8 (1988).
- ⁵¹ O. Eriksson, B. Johansson, and M. S. S. Brooks, *Journal of Physics: Condensed Matter* **1**, 4005 (1989).
- ⁵² V. Sechovsky, L. Havela, F. R. de Boer, P. A. Veenhuizen, K. Sugiyama, T. Kuroda, E. Sugiura, M. Ono, M. Date, and A. Yamagishi, *Physica B: Condensed Matter* **177**, 164 (1992).
- ⁵³ A. V. Andreev, L. Havela, V. Sechovsky, M. I. Bartashevich, T. Goto, and K. Kamishima, *Journal of Magnetism and Magnetic Materials* **169**, 229 (1997).
- ⁵⁴ V. Sechovsky and L. Havela, "Chapter 1 magnetism of ternary intermetallic compounds of uranium," in *Handbook of Magnetic Materials*, Vol. Volume 11, edited by K. H. J. Buschow (Elsevier, 1998) pp. 1–289.
- ⁵⁵ E. Colineau, J. C. Griveau, R. Eloirdi, P. Gaczynski, S. Khmelevskiy, A. B. Shick, and R. Caciuffo, *Physical Review B* **89**, 115135 (2014).
- ⁵⁶ A. J. Millis, S. Sachdev, and C. M. Varma, *Physical Review B* **37**, 4975 (1988).
- ⁵⁷ P. J. Hirschfeld, P. Wolfe, and D. Einzel, *Physical Review B* **37**, 83 (1988).
- ⁵⁸ E. Slooten, T. Naka, A. Gasparini, Y. K. Huang, and A. de Visser, *Physical Review Letters* **103**, 097003 (2009).
- ⁵⁹ E. Miranda, V. Dobrosavljevic, and G. Kotliar, *Physical Review Letters* **78**, 290 (1997).